

가 (skull) 가 (scintigraphy) 가
가 가 가 (thyroxine)
가 가 가 가
가 가 가 가 [1].
가 가 가
(hyperparathyroidism) (medullary thyroid carcinoma)
1. 7.0~10 MHz 가 (sector) (linear array transducer)
49.5% 가
가 2% 4% (sternal notch) [1, 2].
1.5 cm 가
(color Doppler) 가 [3].
CT MRI 가

가 가 .
가 가

가 mm 가 가
, [1, 9, 11].

가 30% (colloid nodule)

가

가

가

가

[1, 4].

(sclerotherapy) 가
Livraghi 101
18.4%
, 33.7% [5].

[illegible]

(multiple endocrine syndrome) 2 가

body)
(medullary thyroid carcinoma)
(foci)
(acoustic shadowing)

[illegible]

(peripheral sonolucent halo): 60~80%, 44% (isoechoic)가 52%, 가
 15% 가 12 가 4 가
 (infarct)
 가 가 가
 가 가
 가 가
 [1, 8].
 가 55~80%
 (follicular) (mixed papillary follicular) (follicular) (follicular carcinoma)
 5~15% 5%
 (calcitonin)
 [1].
 (papillary carcinoma) (psammoma body) (ground glass) (fibrovascular papillary stroma) (branching pattern) (encapsulation) (anaplasia) (lymph node)
 50% 4~7% 90% 10% 20
 (Fig. 1).
 (follicular carcinoma) 가 2~10% 가
 (anaplastic carcinoma) 가 37% 가 가
 18% 가 84%
 1/3 80%
 (medullary carcinoma) (parafollicular) C (branchial pouch) 가 (ultimobranchial body) (thyrocalcitonin) C
 가 (medullary carcinoma) 가 가 CT MRI
 50% 10~20% (pheochromocytoma), (parathyroid adenoma) (hyperplasia) 2 [1].
 (lymphoma) 80% 20%

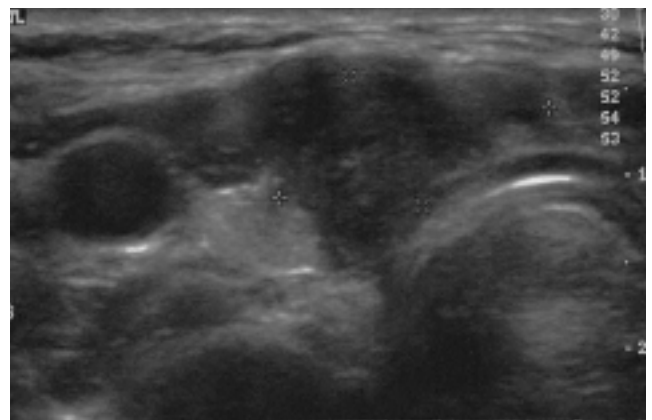


Fig. 1. Papillary thyroid carcinoma. Transverse sonographic scan shows a low echoic solid nodule which has the irregular margin with extracapsular extension and microcalcification.

(Hashimoto's thyroiditis) (Fig. 2).
 B (adenoma), (nodular hemorrhage), (degenerated)
 (granulomatous disease) (follicular adenoma)
 CT (Hürthle cell adenoma) 3 cm
 (Plummer's disease)
 (thyroid suppression test) (cystic degeneration)
 (hyperthyroidism) 2% (sonic transmission) 가
 10 가 cyst) 가가 (colloid)
 45 가 가 (Graves' disease) (multinodular goiter)
 가 (exophthalmus) 가
 0.15~0.5% 가 (tracheoesophageal compression) 가 가
 65 3~5% 3%
 가 가 10-15% 40~60 가
 가 4~6 (Hashimoto's thyroiditis) 가 [1].
 (iodine) (suppurative thyroiditis)
 (dietary goitrogen) (Streptococcus)

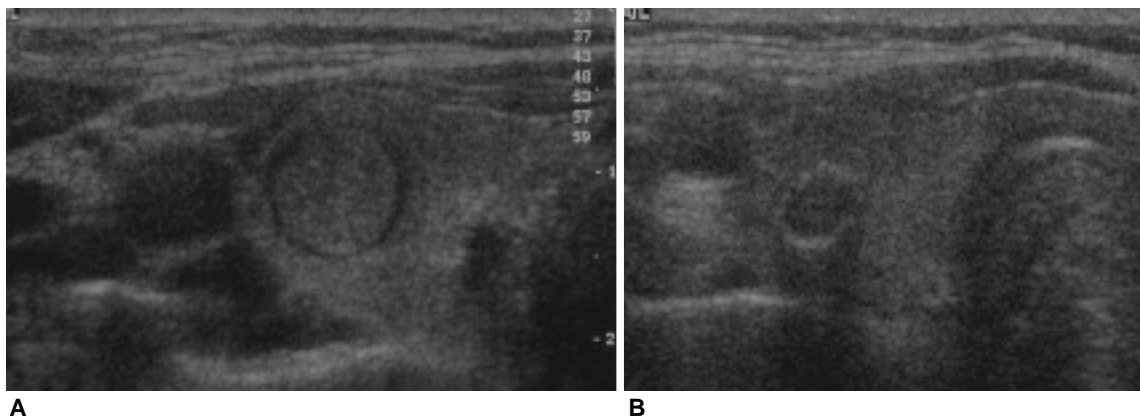


Fig. 2. Benign thyroid nodules.

A. On transverse scan, the isoechoic solid nodule has a perinodular halo with the thin continuous low echoic rim. **B.** The benign thyroid nodule has egg-shell calcification with posterior shadowing.

:
 (mediastinum), (pericardium) (neck)
 가 (branchial cleft anomaly) 4 가
 (cricothyroid junction) 가 [10].
 (Hashimoto's thyroiditis) 가
 5~10 가
 가 가 40~60 가
 6 50% 1.5 cm 가 1 gm 90%
 (chief cell) 5% 가 (Fig. 3).
 (lipoadenoma) 가
 가
 (Riedel's thyroiditis) 가
 , , 가
 CT 20% 가
 (incidentaloma) 가 0.5%
 (retroperitoneal fibrosis),
 (mediastinal fibrosis), (sclerosing
 cholangitis) 가 (orbital pseudotumor)
 (de Quervain's thyroiditis)
 (Coxsackie virus),
 (adenovirus), , ECHO
 (mumps virus) 가
 [1].
 2. (Parathyroid gland)
 4
 (hyperpara - thyroidism)
 (hyperplasia) [9].
 4 2 8
 3 가 (branchial pouch)
 (parathyroid adenoma)
 (parathyroid hyperplasia) 가
 1.5 cm 가 1 gm 90%
 (chief cell) 5% 가 (Fig. 3).
 (lipoadenoma) 가
 가
 CT 20% 가
 (incidentaloma) 가 0.5%
 (percutaneous ethanol ablation)
 1 - 2
 (parathyroid hormone) 가 [11].
 MIBI 가 가
 (localization technique)
 가 91.8%, (hyperplasia) 61.7%, (ectopic
 adenoma) 92.6%
 MIBI
 MIBI
 가 (false positive)
 [9].
 3. (salivary gland)
 가
 (parotid gland) (serous gland)
 [12].
 (secretory duct)
 (Stensen's duct) 3 mm

가 4cm 가
 (masseter) (cheek)
 (buccal space) 가 (buccinator muscle)
 2 (molar)
 (papilla) (Wharton's duct)
 3 mm 가 4 cm
 (mylohyoid muscle)
 가 (sublingual gland)
 (mouth floor) (sublingual papilla)
 (Fig. 4). (minor salivary gland)
 (palate), (paranasal sinus), (pharynx),
 (larynx)
 가 가
 가 가
 (deep lobe)
 (retromandibular vein)
 (external carotid
 artery)
 (pretragal node)
 (pleomorphic adenoma)
 (tumor seeding) 가 , 가 (false
 negative rate),
 (sialoceles)
 (sialolithiasis)
 1.2%
 80~92% 6 - 19%
 1 - 2% . 75%가
 가 3% . 1cm

(sialography) (Dormian basket)
 (radioopaque) 85%가
 (Wharton's duct) 15% (hilum)
 가 35% (ostium)
 30% . 94% 가
 61% (Fig. 5).
 (megaduct) [13].
 (sialadenitis)
 가 (mumps)
 (influenza),

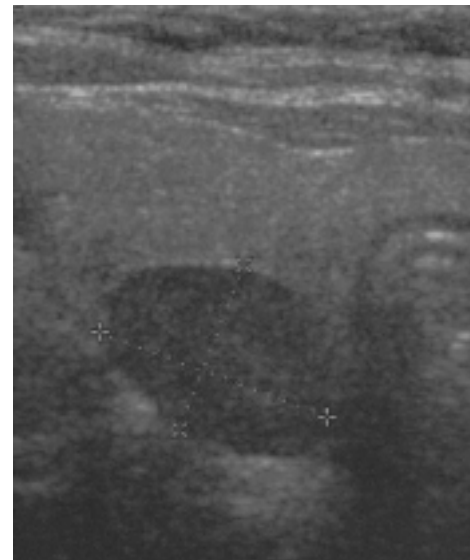
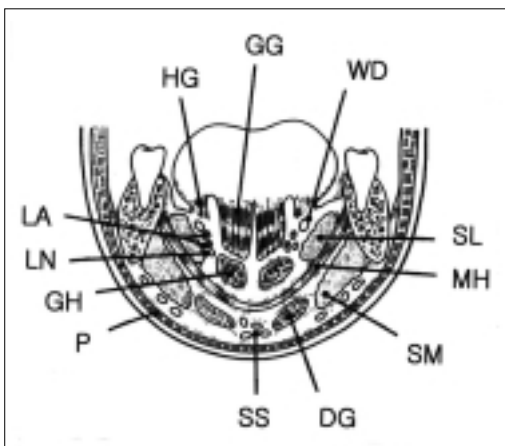
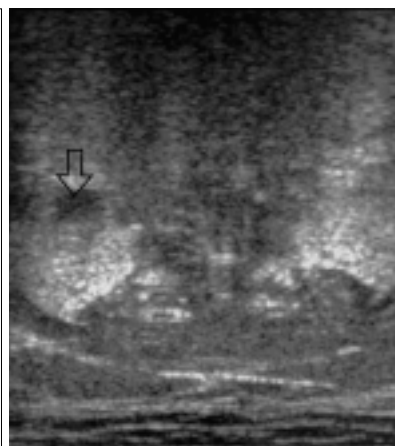


Fig. 3. Parathyroid adenoma with hyperparathyroidism. Transverse ultrasonographic scan shows a solid oval mass posterior to the thyroid.



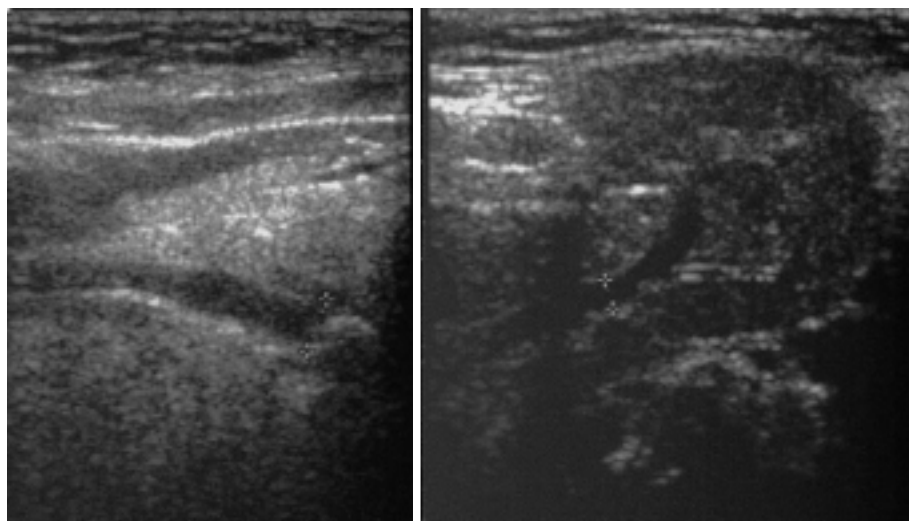
A



B

Fig. 4. The tongue and mouth floor. **A.** Diagram shows cross-cut anatomy of the tongue and mouth floor. DG: anterior belly of the diaphragm muscle, GG: genioglossus, GH: geniohyoid, HG: hyoglossus, LA: lingual artery and vein, LN: lingual nerve, MH: mylohyoid, P: platysma, SL: sublingual gland, SM: submandibular gland, SS: submental space, WD: Wharton's duct. **B.** Ultrasonography shows transverse scan of the mouth floor at the same plane as the previous diagram (A). This patient shows dilatation of the right Wharton's duct (open arrow) due to the distal duct stone.

(Coxsackie A), (echovirus), (sicca)
 (cytomegalovirus), (Ebstein - 가 가
 Barr virus) 5 - 10%
 (chronic recurrent parotitis)
 (periacinar lymphocytic infiltration) 88%
 (microcytic ductal dilatation) 33% 가
 2 - 4 mm 2 - 5 mm
 (Fig. 5). (acinar ectasia) 43% (Fig. 6).
 (lymphocytic infiltration) 가 76 - 88%
 (sarcoidosis) 80%, 50% 가
 10 - 30% 100% (lym -
 83% phoepithelial cyst) [12].
 (caseation) 86%
 (toxoplasmosis), - (lymphoepithelial cyst)
 (cat - scratch disease) (actinomycosis) HIV
 HIV
 (Sjögren 's syndrome) 20 - 80% 가 30% 50%
 가 가 가
 가 (connective tissue disease) (Sjögren 's syndrome)
 40 - 60 (Warthin 's tumor)
 (90%).
 (myoepithelial islets)
 (intercalated duct)
 가 (psudocystic acini) 가 1 가 (first branchial anlomaly)
 (parenchymal cavity) (cyst) 가



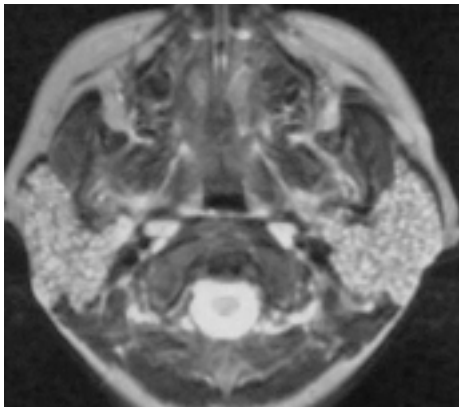
A

B

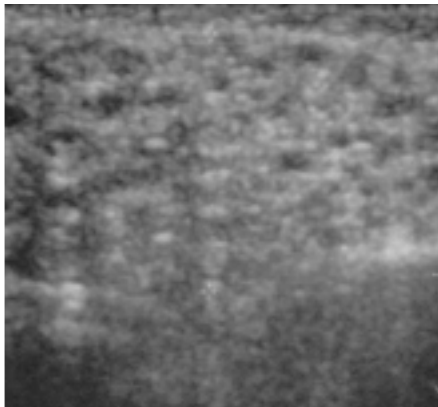
Fig. 5. Sialithiasis.

A. On the oblique longitudinal scan, a s-
 tone is impacted in the Wharton 's duct
 near the orifice with dilatation of the
 proximal duct. **B.** Submandibular gland
 shows chronic sialadenitis which has
 the contracted gland with diffuse low e-
 cho with dilatation of the Wharton 's
 duct (diameter over 4 mm).

(fistula)		(hyoid)	
가			
(Fig. 7).		(tract)	
가			
(dermoid cyst)			
		(pleomorphic adenoma)	
		(mixed tumor)	
		(epithelial component)	(myxoid),
		(chondroid),	(osteoid)
		(myoepithelial)	
(sialoceles)			
		84%,	8%,
			90%
			6.5%,
			0.5%
(retention cyst)		가	가
(buccolingual accessory gland)		(posterior enhancement)	
		25%	
		(satellite nodule)	
(simple ranula)			
(plugging ranula)	가		
(Fig. 8).			
/ (epidermoid/dermoid cyst),		가	
(thyroglossal duct cyst),		5 - 10	3 - 13%가
(cystic		25%	(carcinoma
hygroma)		ex pleomorphic adenoma).	
		가	[14].
(polycystic disease of the parotid)			



A

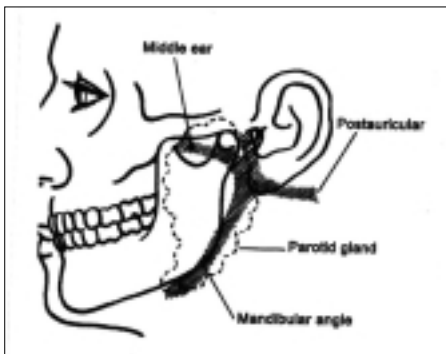


B

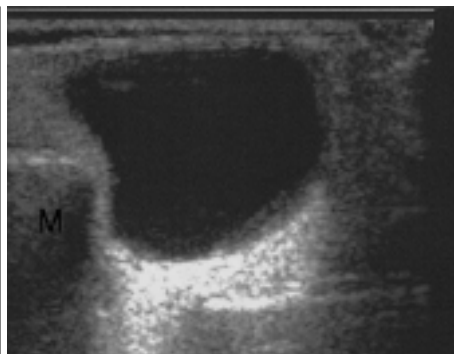
Fig. 6. Sjögren's syndrome.

A. T2 weighted MR image shows enlargement of the bilateral parotid glands with numerous high intensities.

B. Ultrasonography shows numerous hypoechoic nodules in the whole gland parenchyma with mild dilatation of Stensen's duct.



A



B

Fig. 7. First branchial arch anomaly.

A. Distribution of first branchial anomaly is from the external auditory canal superiorly down to the hyoid bone inferiorly.

B. An oval shaped cyst has the thin wall in the superficial lobe of the parotid gland (M: mandibular ramus).

(basal cell adenoma) 2% (duct) 40 (tail) 5 - 15%

가 (adenoid cystic carcinoma) 가 ,

(oncocytoma) (oxyphilic granular cell adenoma) vascularity) 가 (Fig. 9). (hilar type) (central

가 (Warthin's tumor) 가 (uptake) 가 (branchial cyst)

(Warthin's tumor) 6~10% (nerve sheath tumor) 가 (schwannoma)

(papillary cystadenolymphoma) (cystic change)가 (Fig. 10).

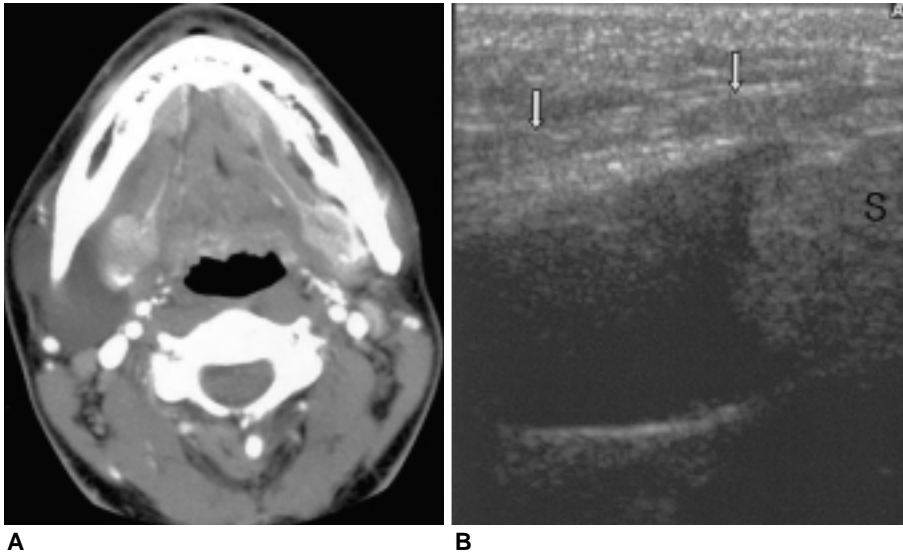


Fig. 8. Plunging ranula.
A. Contrast enhanced-axial CT shows fluid collection around the submandibular gland. **B.** Cyst-like lesion dives into the right submandibular space from the sublingual space (S:submandibular gland, arrows: mylohyoid muscle).

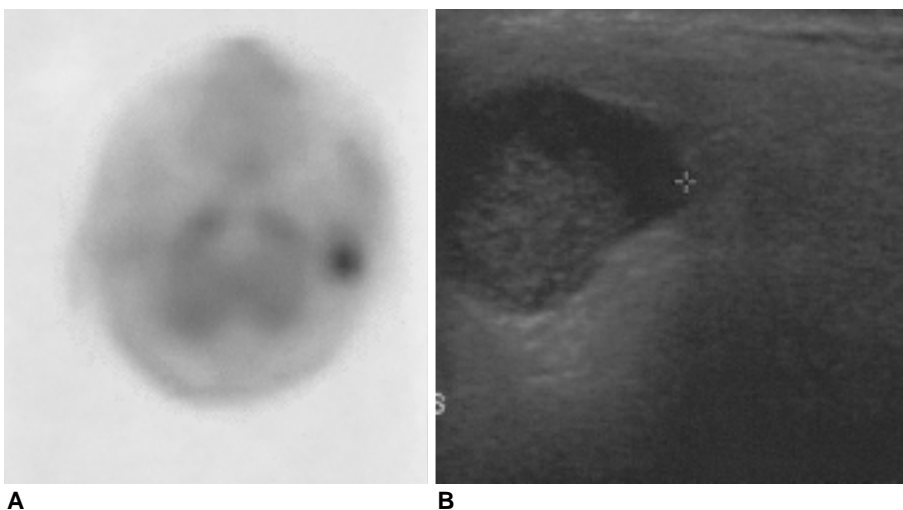


Fig. 9. Warthin's tumor.
A. FDG PET show hypermetabolic spot in the left parotid area. **B.** Transverse ultrasound shows oval shaped mass with heterogeneously low echogenicity in the parotid tail.

(neurofibromatosis) 1 가 (stylomastoid) [15]. (acinic cell tumor) 2 - 4%
 15 - 17% 가 2가 가
 (granular cell) (clear cell) 가
 20%, 60%, 가 30~35% 가
 80% 가 가
 (lymphoma)
 (mucoepidermoid carcinoma) 30% 가
 50% 50%가
 (buccal mucosa) 1 - 8%
 (low malignancy) 80% 가 가
 가 [3]. 12 - 14%가
 (Warthin ' (acinic cell tumor),
 (adenoid cystic carcinoma) s tumor),
 4 - 15% , 15% , 25 - (pleomorphic adenoma), (oncocytoma),
 2 - 6% , 15% , 15% 가 가
 31% 가 가
 40 가 가
 (perineural invasion) (mucoepidermoid),
 (phlebolith)

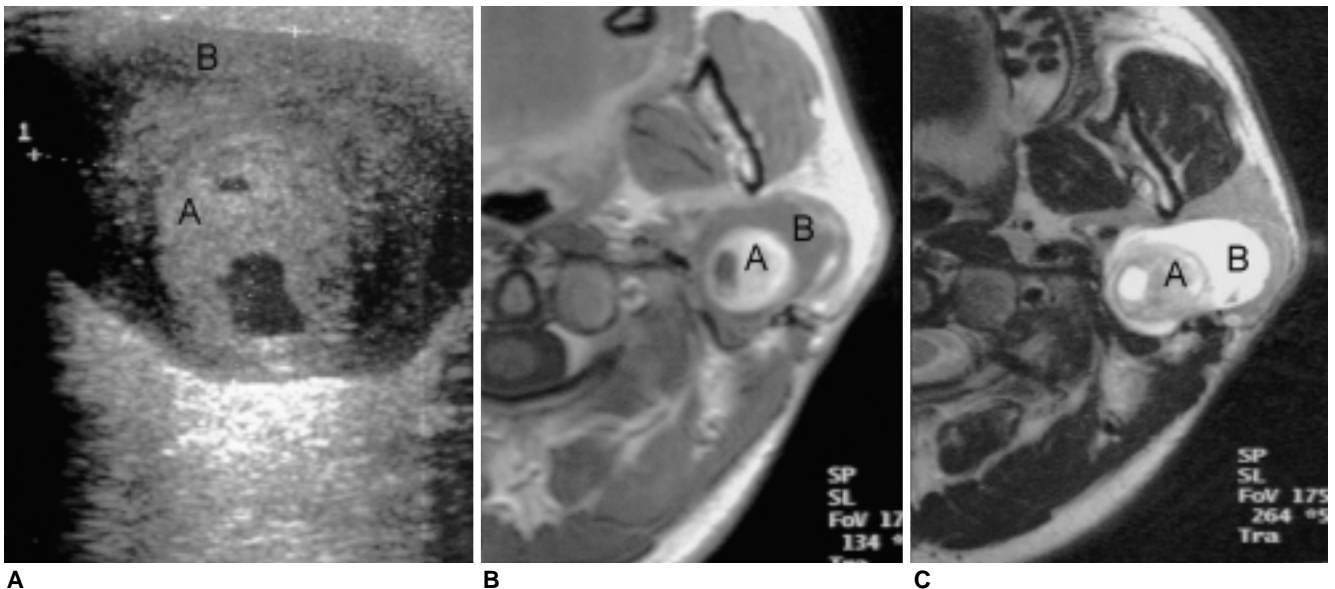


Fig. 10. Facial nerve schwannoma.

A. T2 weighted image shows the parotid mass with two components of which the former is the Antoni type A, compacted component with higher cellularity and the latter is Antoni B component, loose one with lower cellularity. Note cystic change in the central component. **B.** On gadolinium-enhanced T1 weighted image, the central higher compact component shows the intense enhancement, and the outer loose component shows the less enhancement. **C.** Transverse scan shows these two components seperately.

(Kimura disease)
(eosinophilia)

가

가

(70%).

ular hyperplasia)

(eccentric)

(follic -

(margin): 46%

가

14%

가

가

(imaging - based level nodal classification)

400 - 700

300

가

(nodal echotexture):

25 - 40%

(micro -

metastases)가

1999

(imaging

based nodal classification)

(Fig. 11)

[16].

(parotid node or

retropharyngeal node)

(keratinized)

(coagulation necrosis)

(caseation necrosis)

24.3%

84%

88%

가 82%

98%, 95%

3~12mm

가 70%

89%

CT MRI

가

PET

가

PET

가

(Warthin's tumor)

1 cm

42%

1 cm

가

longitudinal/largest transverse diameter ratio)

(maximal

L/T 2

81 - 95%

가

67 - 96%

(hilum)

가

가

(76 - 92%)

가

가

가 [17, 18].

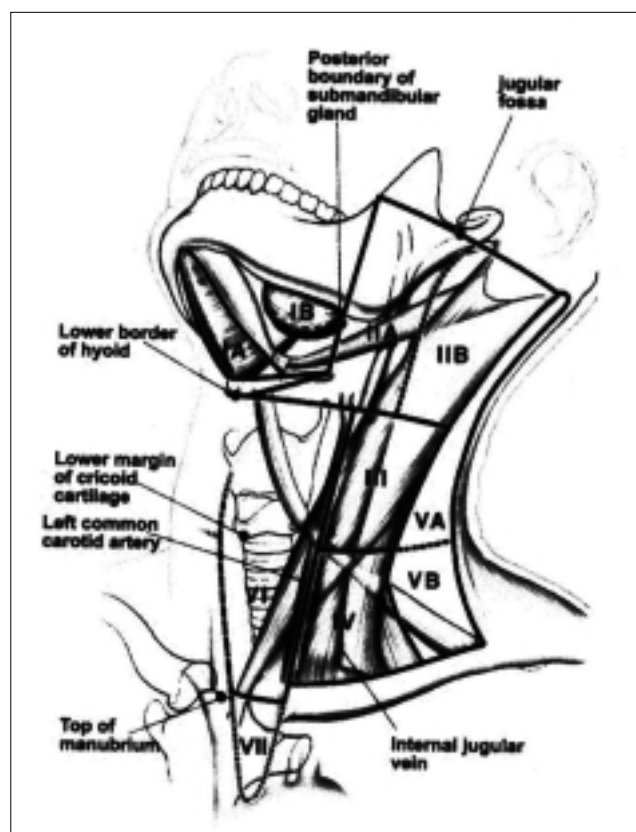


Fig. 11. Diagram of the head and neck viewed from the left oblique anterior projection. The broad lines outline the boundaries of the nodal levels, and I to VII identify the specific nodal levels of the imaging based level nodal classification.

가 (fluid)가 가 (Fig. 12).
가
()
(encasement)
(internal jugular vein)
(Valsalva)
(pulsed Doppler)
Chang 81% RI가 0.6
19% RI가 0.6
가 [19].
power
4 1 (hilar
type), 2 (spotted type), 3
(peripheral type, 4 (mixed type)
83%
78% (non - hilar type)(47%,
20%, 11%) [20].
Steinkamp , ,
(82.1%)
(84.7%).
가 . Wu
(vascular index) 0.048
0.169 가
(positive
predictive value)
가 [21].
4%
가 1/3
1/3
가
가 96% CT MRI
가 69%
가



Fig. 12. Metastatic lymph node from thyroid carcinoma. These level III nodes shows decreased L/T ratio, cluster of multiple lymph nodes, absence of hilar echo and heterogeneous internal echo.

가 (Fig. 13). epithelium) 가 (follicle)가
 가 (melanoma) 1 - 2%가 , 25%가 , 60%가
 가 (pseudohilum) 13 - 14%가 40% 1%
 [17, 23].

(Kikuchi disease: histiocytic necrotizing lymphadenitis)

가
 가 가 [24, 25].
 가 (Fig. 14).
 가

(self - limited).
 가
 2.5 cm
 (posterior triangle) 가
 가 [17].

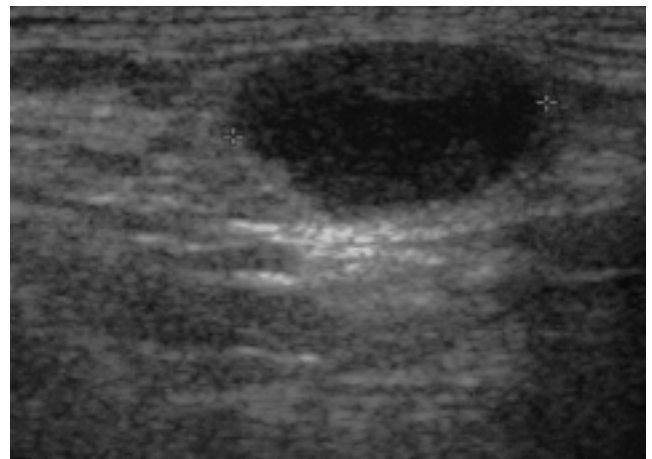


Fig. 13. Tuberculous lymphadenitis. This level V node shows the low internal echo with heterogeneity, slightly decreased L/T ratio without presence of hilar echo.

5. (congenital neck cyst)
 (thyroglossal duct cyst)
 30 83.3%
 (foramen cecum)
 (suprasternal)
 (squamous) (ciliated pseudostratified

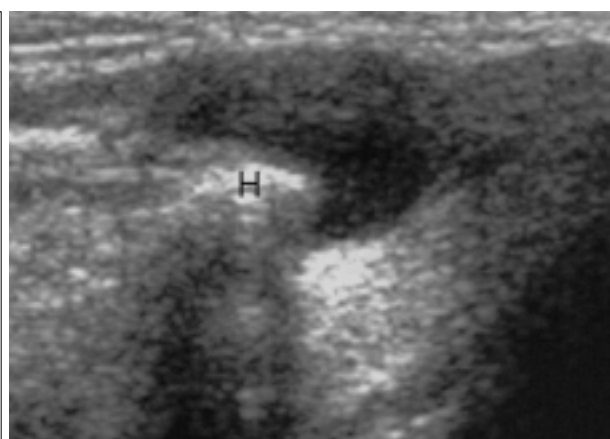
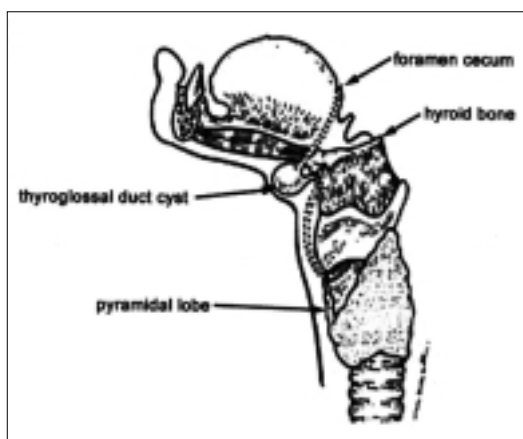
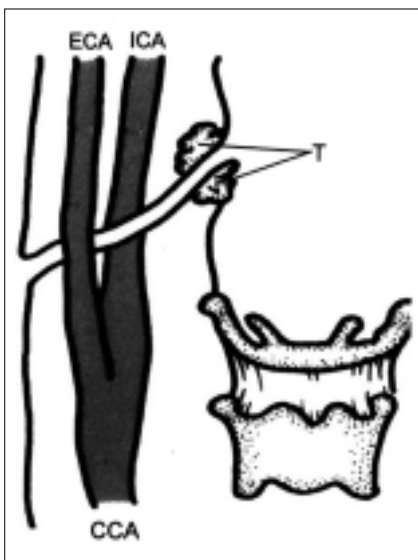


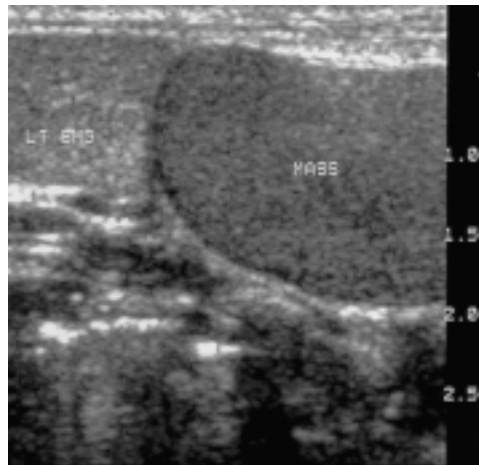
Fig. 14. Thyroglossal duct cyst.
A. The diagram traces the course of the thyroglossal duct cyst from the foramen cecum downward, at first ventral to the hyoid bone and then dorsal to the hyoid. The duct then descends in the neck to the level of the normal thyroid bed, especially pyramidal lobe. **B.** On the midline longitudinal scan, an oval shaped cyst is surrounding the hyoid bone (H). The right of the picture is the feet side.

[24].

가 (branchial anomaly)
가 가 2 가
가 가 80 - 90% 가
(sternocleidomastoid muscle), (thymic cyst), (bronchogenic cyst), (laryngocele)
(fistula) (Fig. 15).
1 가 8% (cystic lymphangioma)
(Fig. 7). 90% 2

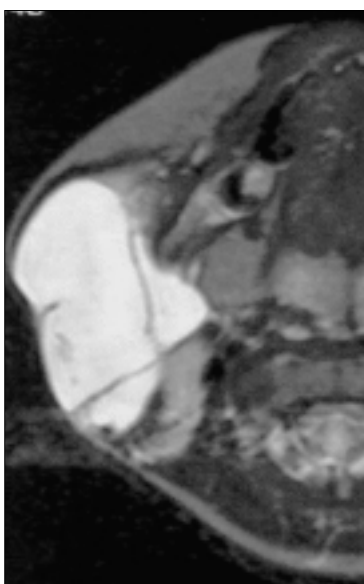


A

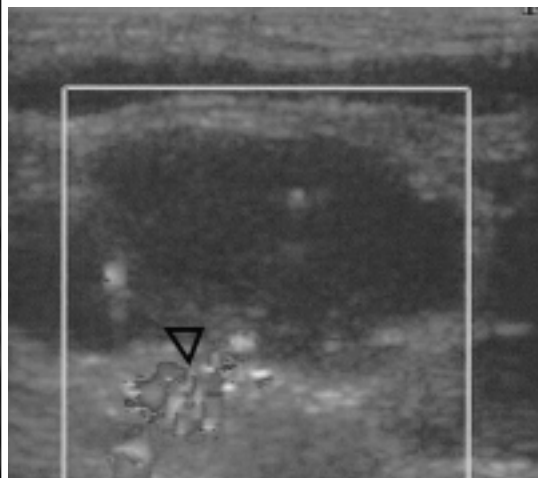


B

Fig. 15. A. Diagram of the course of the second branchial anomaly. The cutaneous opening is located along the anterior border of the sternocleidomastoid muscle. The tract passes through bifurcations between the internal carotid artery (ICA) and external carotid artery (ECA), finally into the palatine tonsil (T) (CCA: common carotid artery). **B.** The oblique scan shows a well defined mass posterior to the submandibular gland (SMG) and anterior to the sternocleidomastoid muscle. It has echogenic contents with coarse echoic debris mimicking solid neoplasm.



A

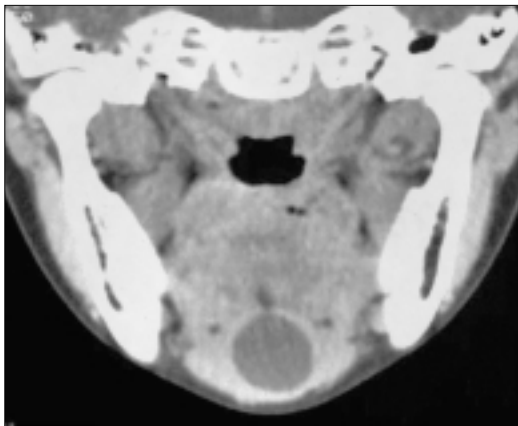


B

Fig. 16. Cystic hygroma with hemorrhage.

A. T2 weighted image shows the multi-septated cystic lesion in the right parotid gland. Hemorrhage is detected in the several cysts. **B.** Color Doppler shows the cyst mixed with several vascular structures (open arrow head).

(sac) (cystic hygroma), (cavernosus) (thymic cyst) (thymopharyngeal duct)
 (capillary) (Fig. 16). 가
 (hemangioma) 가 2 가
 가 dexycycline OK - [26].
 432(picibanil) (sclerotherapy) 가 6. (miscellaneous)
 (epidermoid cyst) (deep neck infection) 가
 20 - 30 (prevertebral)
 (submandibular space) (tonsillitis),
 (peritonsillar inflammation),
 CT (Fig. 17).



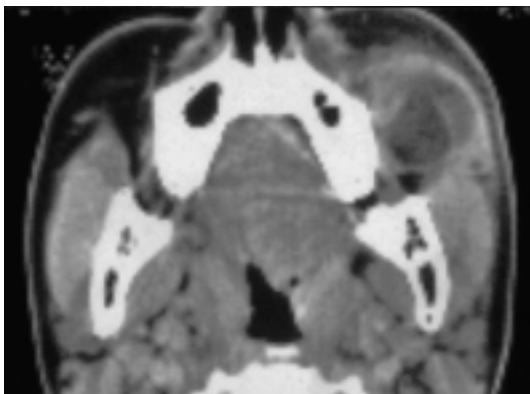
A



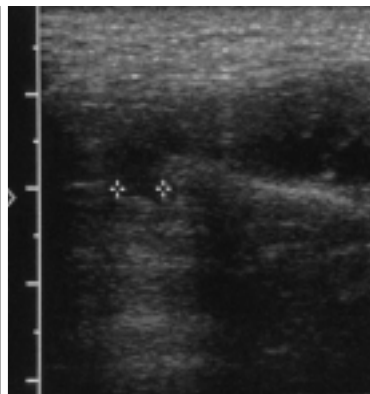
B

Fig. 17. Epidermoid in the sublingual space.

A. Coronal CT shows the spherical cyst in the sublingual space. **B.** Inverted ultrasonographic scan shows low echoic lesion, which is separated from the hyoid bone, with the well defined margin with numerous echogenic foci.



A



B

Fig. 18. Buccal abscess.

A. Axial CT shows abscess in the left buccal space. **B.** Transverse ultrasonography shows fluid collection with widening of the Stensen's duct (criss-crosses). This patient has history of recurrent episodes of buccal infection due to stricture of Stensen's duct.

가
(streptococci) (staphylococci) .
(Fig. 18). [24].
(lipoma)
. 90%
가 CT
가 [27].
(schwannoma)
(schwann)
. 2.5%
가 가
가
(paraganglioma) (Fig. 10).
(neurofibroma)
(endoneurium)
(concentric)
(plexiform)
(neurofibromatosis) 1

(paraganglioma or glomus tumor)
(glomus vagale),
(glomus jugulare), (glomus tympanicum)
. 10% 5%
[24].
(fibromatosis colli)
(sterno -
cleidomastoid muscle)
(torticollis)
가 가 (Fig. 20).
가
(tongue and mouth floor)
가 M -
2 (digstric muscle)
(mylohyoid muscle) (sublingual)
(submandibular)
(lamina propria) 3
X - TV

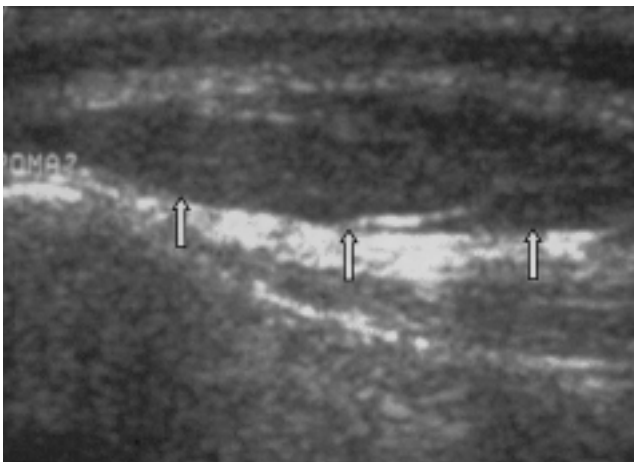


Fig. 19. Lipoma in the posterior triangle shows elliptical solid mass (arrows) with multiple internal echogenic lines parallel to the skin surface.



Fig. 20. Fibromatosis colli. Oblique ultrasonography shows the fusiform enlargement of the sternocleidomastoid muscle with heterogeneous internal echo.

(tongue cancer)

[24].

가

가

가

8 mm

75%

가 8 mm

29.5%

가 (Fig. 21).

가

가

가

[28].

(cervical esophagus)

C5 T5

가

가

5 mm

가

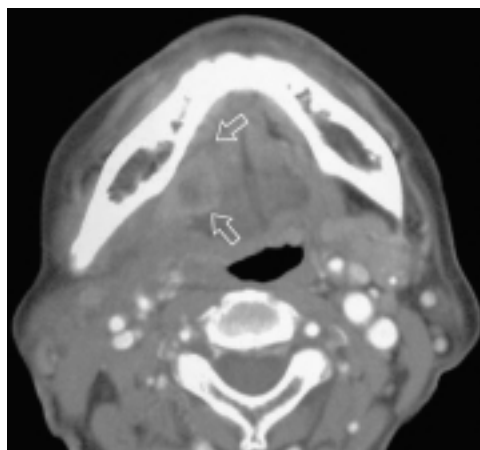
(diverticulum),

(blind area)

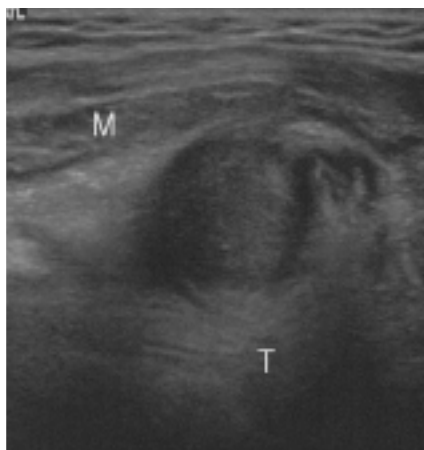
가

. “ E ”

1. Bruneton JN, Livraghi T, Viateau-Poncin J, Leenhardt L, Tramalloni J. Thyroid gland. In: Baert AL and Sartor K, ed. Applications of sonography in head and neck pathology. 1st ed. Berlin: Springer, 2002;1-66
2. Ezzat S, Sarti DA, Cain DR, et al. Thyroid incidentalomas: prevalence by palpation and ultrasonography. Arch Intern Med 1994;154:1838-18402
3. Shimamoto K, Endo TM, Ishigaki T, et al. Thyroid nodules: evaluation with color Doppler ultrasonography. J Ultrasound Med 1993;12:673-678
4. Danese D, Sciacchitano S, Farsetti A, et al. Diagnostic accuracy of



A



B

Fig. 21. Squamous cell carcinoma of the mouth floor.

A. Contrast-enhanced CT shows the ring enhancing lesion in the the mouth floor(open arrows). Note the cancer infiltration to the adjacent soft tissue. **B.** Ultrasonography shows a low echoic solid nodule in the mouth floor(M: mylohyoid, T: tongue).

- conventional versus sonography-guided fine-needle aspiration biopsy of the thyroid nodules. *Thyroid* 1998;8:15-21
5. Livraghi T, Paracchi A, Ferrari C, et al. The treatment of autonomous thyroid nodules with percutaneous ethanol injection: 4-year experience. *Radiology* 1994;190:529-533
 6. Cho YS, Lee HK, Ahn IM, et al. Sonographically guided ethanol sclerotherapy for benign thyroid cysts: results in 22 patients. *AJR Am J Roentgenol* 2000;174(1):213-216
 7. Kim JH, Lee HK, Lee JH, Ahn IM, Choi CG. Efficacy of sonographically guided percutaneous ethanol injection for treatment of thyroid cysts versus solid thyroid nodules. *AJR Am J Roentgenol* 2003;180(6):1723-1726
 8. Kim EK, Park JS, Chung WY, Oh KG, Kim DI, Lee JT, and Yoo HS. New sonographic criteria for recommending fine-needle aspiration biopsy of nonpalpable solid nodules of the thyroid. *AJR Am J Roentgenol* 2002;178:687-691
 9. Poncin J, Lencene RL, Meloni F. Parathyroid gland. In: Baert AL and Sartor K, ed. *Applications of sonography in head and neck pathology*. 1st ed. Berlin: Springer, 2002;67-90
 10. Randel SB, Gooding GA, Clark OH, et al. Parathyroid variants: US evaluation. *Radiology* 1987;165:191-194
 11. Koslin DB, Adams J, Anderson P, et al. Preoperative evaluation of patients with primary hyperparathyroidism: role of high-resolution ultrasound. *Laryngoscope* 1997;107(9):1249-1253
 12. Raffaelli C, Amoretti N, Carlotti B. Salivary gland. In: Baert AL and Sartor K, ed. *Applications of sonography in head and neck pathology*. 1st ed. Berlin: Springer, 2002;91-136
 13. Yoshimura Y, Inoue Y, Odagawa T. Sonographic examination of sialolithiasis. *J Oral Maxillofac Surg* 1989;47(9):907-912
 14. Schick S, Steiner E, Gahleiter A, et al. Differentiation of benign and malignant tumors of the parotid gland: value of pulsed Doppler and color Doppler sonography. *Eur Radiol* 1998;8(8):1462-1467
 15. , , . MR : 2 . 2001;20 (1):77 - 80
 16. Som PM, Curtin HD, Mancuso AA. An imaging-based classification for the cervical nodes designed as an adjunct to recent clinically based nodal classifications. *Arch Otolaryngol Head Neck Surg* 1999;125(4):388-396
 17. Bruneton JN, Matter D, Lassau N, Dassonville O. Lymph nodes. In: Baert AL and Sartor K, ed. *Applications of sonography in head and neck pathology*. 1st ed. Berlin: Springer, 2002;137-164
 18. Vassallo P, Wernecke K, Roos N, et al. Differentiation of benign from malignant superficial lymphadenopathy: the role of high-resolution US. *Radiology* 1992;183:215-220
 19. Chang DB, Yuan A, Yu CJ, et al. Differentiation of benign and malignant cervical lymph nodes with color Doppler sonography. *AJR Am J Roentgenol* 1994;162:965-968
 20. Wu CH, Hsu MM, Chang YL, Hsieh FJ. Vascular pathology of malignant cervical lymphadenopathy: qualitative and quantitative assessment with power Doppler ultrasound. *Cancer* 1998;83(6): 1189-1196
 21. Giovagnorio F, Rusticali A, Araneo AL. Color and pulsed Doppler evaluation of benign and malignant adenopathy. *Clin Imaging* 1997;21:163-169
 22. Steinkamp HJ, Cornehl M, Hosten N, et al. Cervical lymphadenopathy: ratio of long- to short-axis diameter as a predictor of malignancy. *Br J Radiol* 1995;68:266-270
 23. Ying M, Ahuja AT, Evans R, et al. Cervical lymphadenopathy sonographic differentiation between tuberculous nodes and nodal metastases from non-head and neck carcinoma. *J Clin Ultrasound* 1998;26:383-389
 24. Bruneton JN, Tranquart F, Brunner P, Mourou MY. Miscellaneous. In: Baert AL and Sartor K, ed. *Applications of sonography in head and neck pathology*. 1st ed. Berlin: Springer, 2002;253-286
 25. , , 4 . : 2001;44(1):1-6
 26. Som PM, Smoker WRK, Curtin HD. Congenital lesions. In Som P and Curtin HD, ed. *Head and neck imaging*. 4th ed. St. Louis: Mosby, 2003;1835-1836
 27. Ahuja AT, King AD, Kew J, et al. Head and neck lipomas: sonographic appearance. *AJNR Am J Neuroradiol* 1998;19:505-508
 28. Gritzmam N, Hollerweger A, Macheiner P, Rettenbacher T. Sonography of soft tissue masses of the neck. *J Clin Ultrasound*. 2002;30(6):356-373